ADVANCED OPTICAL MATERIALS
www.advopticalmat.de

Highly Scalable, Wearable Surface-Enhanced Raman Spectroscopy

Limei Liu, Pablo Martinez Pancorbo, Ting-Hui Xiao, Saya Noguchi, Machiko Marumi, Hiroki Segawa, Siddhant Karhadkar, Julia Gala de Pablo, Kotaro Hiramatsu, Yasutaka Kitahama, Tamitake Itoh, Junle Qu, Kuniharu Takei, and Keisuke Goda**

The last two decades have witnessed a dramatic growth of wearable sensor technology, mainly represented by flexible, stretchable, on-skin electronic sensors that provide rich information of the wearer's health conditions and surroundings. A recent breakthrough in the field is the development of wearable chemical sensors based on surface-enhanced Raman spectroscopy (SERS) that can detect molecular fingerprints universally, sensitively, and noninvasively. However, while their sensing properties are excellent, these sensors are not scalable for widespread use beyond small-scale human health monitoring due to their cumbersome fabrication process and limited multifunctional sensing capabilities. Here, a highly scalable, wearable SERS sensor is demonstrated based on an easy-to-fabricate, low-cost, ultrathin, flexible, stretchable, adhesive, and biointegratable gold nanomesh. It can be fabricated in any shape and worn on virtually any surface for label-free, large-scale, in situ sensing of diverse analytes from low to high concentrations (10–$10^6 \times 10^{-9}$ M). To show the practical utility of the wearable SERS sensor, the sensor is tested for the detection of sweat biomarkers, drugs of abuse, and microplastics. This wearable SERS sensor represents a significant step toward the generalizability and practicality of wearable sensing technology.

1. Introduction

The last two decades have witnessed a dramatic growth of wearable sensor technology, mainly represented by flexible, stretchable, on-skin electronic sensors that provide rich information of the wearer's health conditions and surroundings.[1,2] Current wearable sensors generally track the wearer's motions and vital signs, such as steps, blood pressure, blood oxygen saturation, respiratory rate, and heart rate, under everyday conditions,[3] and have been recently upgraded to perform in situ chemical sensing of the wearer's biofluids, such as sweat, saliva, tears, and urine, in a noninvasive manner.[4] Multiplexed chemical analysis of biomarkers in biofluids is essential for an accurate and comprehensive understanding of the wearer's complex physiological and pathological conditions.[5] Unfortunately, conventional wearable sensors are only sensitive to one

L. Liu, P. Martinez Pancorbo, T.-H. Xiao, S. Noguchi, M. Marumi, S. Karhadkar, J. Gala de Pablo, K. Hiramatsu, Y. Kitahama, K. Takei, K. Goda
Department of Chemistry
The University of Tokyo
Tokyo 113-0033, Japan
E-mail: xiaoth@chem.s.u-tokyo.ac.jp; goda@chem.s.u-tokyo.ac.jp

L. Liu
College of Mechanical Engineering
Yangzhou University
Yangzhou 225127, China

L. Liu, J. Qu
College of Physics and Optoelectronic Engineering
Shenzhen University
Shenzhen 518060, China

The ORCID identification number(s) for the author(s) of this article can be found under https://doi.org/10.1002/adom.202200054.

DOI: 10.1002/adom.202200054

T.-H. Xiao, K. Goda
Institute for Quantum Life Science
National Institute for Quantum and Radiological Science and Technology
Chiba 263-8555, Japan

H. Segawa
Third Department of Forensic Science
National Research Institute of Police Science
Chiba 277-0882, Japan

T. Itoh
Health and Medical Research Institute
National Institute of Advanced Industrial Science and Technology
Takamatsu 761-0395, Japan

K. Takei
Department of Physics and Electronics
Osaka Metropolitan University
Osaka 599-8531, Japan

K. Goda
Institute of Technological Sciences
Wuhan University
Hubei 430072, China

K. Goda
Department of Bioengineering
University of California
Los Angeles, CA 90095, USA

type of chemical in an analyte at a time and need to be tailored for the target analyte due to their limited sensing mechanism (mainly originating from the electronic nature of the sensors). For this reason, they are incapable of distinguishing different chemicals simultaneously in a single measurement.[6] Alternatively, they can be designed to measure multiple chemical species, but these modifications lead to larger sizes, higher fabrication costs, more synthetic steps, and the need for prior knowledge of the target analyte.[7]

Surface-enhanced Raman spectroscopy (SERS) has emerged as an attractive approach to next-generation wearable sensors in recent years due to enabling highly sensitive, multiplexed chemical sensing of complex analytes in a noninvasive and label-free manner without the need for prior knowledge of the analytes.[1,8–12] Recently, several groups have achieved significant milestones.[2,13] Specifically, Jeong et al. demonstrated wearable SERS sensors composed of multilayered nanowire arrays by nanotransfer printing techniques.[14,15] Garg et al. demonstrated a semipermeable wearable SERS sensor composed of a micropillar array with self-assembled gold nanoparticles by template-assisted self-assembly and micro/nanoimprinting.[16] Wang et al. developed a wearable SERS sensor composed of a plasmonic metafilm formed by an ordered silver nanocube superlattice.[13] Koh et al. demonstrated a different wearable SERS sensor composed of plasmonic silver nanowires on a silk fibroin protein film.[2] While these SERS sensors show excellent molecular specificity and high detection sensitivity, their scalability remains challenging due to their intricate fabrication processes and limited multifunctional sensing capabilities. They rely on either a low-throughput laser writing method or small-area transfer methods for their fabrication. It is difficult to fabricate the sensors on a large scale (e.g., sensors with a size larger than 10 cm × 10 cm) at a low cost for diverse applications.

In this study, we report our demonstration of a highly scalable wearable SERS sensor based on an easy-to-fabricate, low-cost, ultrathin, flexible, stretchable, adhesive, and biointegratable gold nanomesh (**Figure 1**a,b). This sensor was inspired by a recently reported inflammation-free, gas-permeable, lightweight, stretchable electronic sensor made of gold-coated biocompatible polyvinyl alcohol (PVA) nanofiber that is attachable to human skin or nonflat, nonrigid surfaces for long durations of time.[17] We exploited its undiscovered optical properties and optimized its dimensions to obtain SERS capabilities, while retaining its excellent features such as easy fabrication, cost-effectiveness, thinness, high flexibility, high stretchability, high adhesivity, and high biointegratability (Figure 1c–f). This 2D sensor is moldable and can be fabricated in any shape and worn on virtually any surface for label-free, large-scale, in situ sensing of diverse analytes from low to high concentrations ($(10–10^6) \times 10^{-9}$ M). To show the practical utility of the wearable SERS sensor, we tested the sensor for the detection of sweat biomarkers, drugs of abuse, and microplastics.

2. Results and Discussion

To investigate and optimize the optical properties of the wearable SERS sensor for optimum SERS performance, we performed numerical simulations using COMSOL Multiphysics based on the finite-element method for a gold nanomesh model, as shown in **Figure 2**a (see Supporting Information for details). The gold nanomesh model was adopted to simulate the structure shown in Figure 1f. It is evident from Figure 2b,c that hot spots in each crescent-shaped gold nanowire are mainly localized at the sharp edges of the nanowire without strong structural resonance in the entire nanowire due to its relatively large size. We optimized the number of hot spots in a unit volume by decreasing the diameter of the nanowire while ensuring its sufficient mechanical strength for wearability. A gold nanowire diameter of 490 nm and a deposited gold thickness of 150 nm were selected as optimum geometric dimensions (see Figure S1 in the Supporting Information for more details). As shown in Figure 2d,e, the dependence of the maximum local electric-field enhancement and absorption spectrum of the gold nanomesh model on the gap size between nanowires indicates high SERS performance and optimum excitation wavelength (about 785 nm).

As a proof-of-principle demonstration of the wearable SERS sensor's ability to detect molecules with high sensitivity, we used it to conduct SERS of rhodamine 6G (R6G) solutions on the sensor. With an integration time of 20 s and an excitation power of 2 mW at an excitation wavelength of 785 nm, we first measured the Raman spectrum of an R6G solution at a concentration of 0.1 M on a silicon substrate as the ground truth. The characteristic Raman peaks of R6G were observed, as shown in **Figure 3**a. Then, by decreasing the laser excitation power to 0.2 mW and the R6G concentration to 100×10^{-9} M, we observed the disappearance of the Raman spectrum on both the silicon and 150 nm thick gold film substrates as expected. On the other hand, the Raman spectrum was visible on the wearable SERS sensor under the same conditions under the Raman signal enhancement. The SERS enhancement factor was found to be (2 mW/0.2 mW) × (1 M/100×10^{-9} M) × (0.8 a.u./0.45 a.u.) ≈ 10^8 for R6G (see the Supporting Information for details). It is important to mention that the enhanced Raman spectrum measured on the wearable SERS sensor agrees with the ground truth. Figure 3b,c shows that the lowest detectable concentration of R6G is about 10×10^{-9} M (see Movie S1 in the Supporting Information for our demonstration of Raman spectroscopy on the wearable SERS sensor).

Furthermore, to show the flexibility of the wearable SERS sensor as a SERS substrate, we conducted a crumpling test by adhering it to a hand glove and opening and closing the hand multiple times. As shown in Figure 3d,e, the Raman spectrum of R6G exhibited no appreciable change even after 1000 crumpling cycles. Likewise, we also performed a stretchability test on the wearable SERS sensor by adhering it to a 50% prestretched polydimethylsiloxane (PDMS) substrate and releasing/stretching it multiple times. As shown in Figure 3f,g, the Raman spectrum of R6G exhibited no appreciable change even after 1000 stretching cycles (50% strain). These results firmly demonstrate the user-friendliness and practical usability of the wearable SERS sensor.

To show the diverse utility of the wearable SERS sensor for SERS applications, we demonstrated high intrinsic adhesivity without using any glues by placing it on the surfaces of various materials such as metals, plastics, fabrics, and organics. **Figure 4**a–c shows the wearable SERS sensor adhered to a human wrist for the detection of sweat biomarkers. The

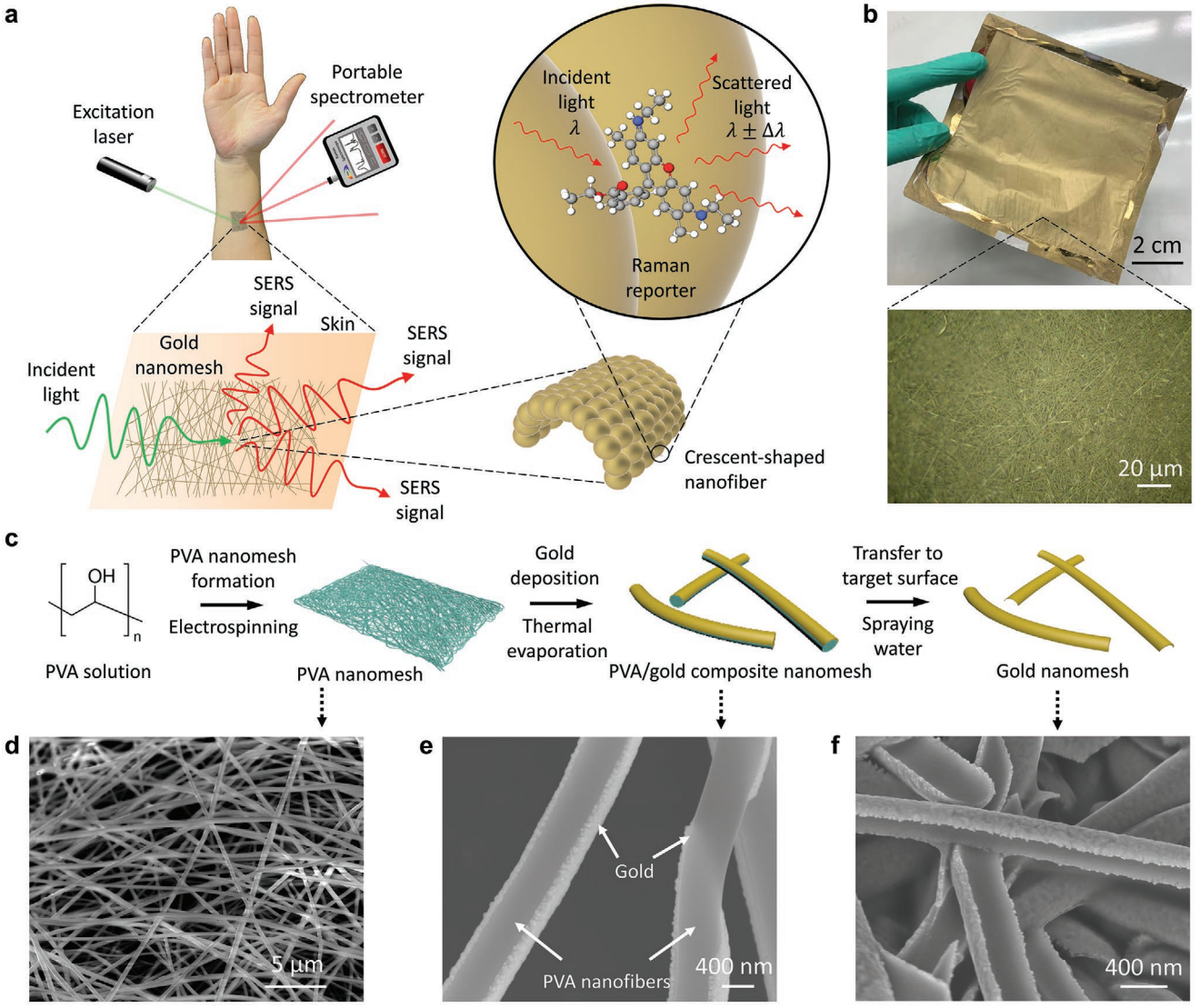

Figure 1. Concept, fabrication, design, and characterization of the wearable SERS sensor. a) Concept of wearable SERS on the skin. b) Picture of the fabricated gold nanomesh. The inset shows a 50× optical microscopy image of the gold nanomesh. c) Fabrication process, and its corresponding SEM images of the gold nanomesh: d) PVA fiber nanomesh, e) gold-coated PVA fiber nanomesh, and f) gold nanomesh after removing the PVA fiber nanomesh.

pictures show that it was firmly attached to the skin even under normal flexion and extension conditions, demonstrating high flexibility, stretchability, adhesivity, and biointegrability. No obvious side effect on the human skin was observed by virtue of the inflammation-free and gas permeable properties of the gold nanomesh[17] (see the Supporting Information about the safety of using the wearable SERS sensor on the human skin). Figure 4d,e shows that the wearable SERS sensor adhered to a human cheek and a contact lens for the detection of biomarkers in tears.[18,19] Similarly, Figure 4f shows the wearable SERS sensor adhered to the surface of a face mask for the detection of breath and saliva biomarkers highly relevant to COVID-19 and other respiratory and oral diseases.[20–24] Figure 4g–i shows the wearable SERS sensor adhered to metallic and plastic surfaces, such as an elevator control panel, a door handle, a doorknob, and a computer keyboard, exhibiting its potential to serve as an environmental monitoring and infection surveillance tool in smart cities.[25] It is worthwhile to note that the wearable SERS sensor can be integrated onto the surfaces of nonwater-resistant objects, such as the computer keyboard, as long as the water amount and sprayed region are well controlled. Moreover, an air dryer can be used to dry the surfaces after the integration. Finally, Figure 4k,i shows the wearable SERS sensor adhered to an apple and a leaf for food safety applications.[1,26,27] To show the practical utility of the wearable SERS sensor, we demonstrate three applications, namely sweat biomarker detection, drug identification, and microplastic detection.

To demonstrate the capability of the wearable SERS sensor for health monitoring as a potential application, we measured human sweat from a human subject as well as two human sweat biomarkers: urea and ascorbic acid. The human sweat sample contains various substances such as sodium chloride, ascorbic acid and urea. **Figure 5**a presents the Raman spectra of 2 μL human sweat obtained from the participant on the

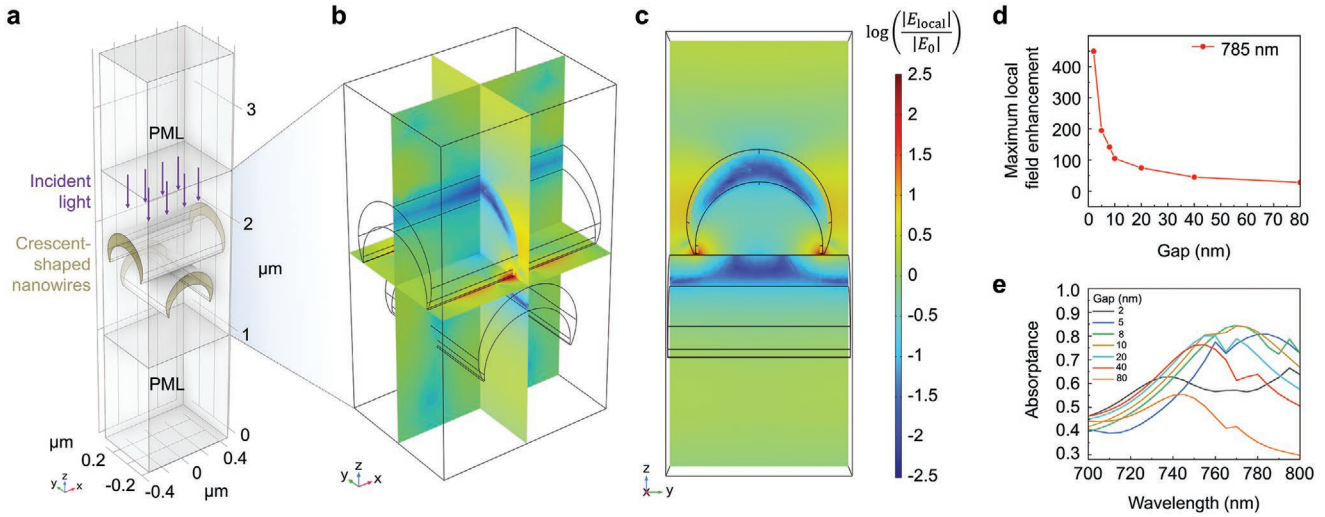

Figure 2. Numerical simulations of the wearable SERS sensor using COMSOL Multiphysics based on the finite-element method. PML: perfectly matched layer. a) Geometrical configuration of a gold nanomesh model composed of two perpendicularly stacked gold nanowires to simulate the wearable SERS sensor. b) Heat map of the centered cross-sections using log ($|E_{local}|/|E_0|$) in three spatial dimensions at an excitation wavelength of 785 nm. c) Heat map of the centered YZ plane cross-section using log ($|E_{local}|/|E_0|$) at the same excitation wavelength. d) Maximum local electric-field enhancement as a function of the gap between nanowires from the heat map simulation in a nonlogarithmic representation. e) Absorptance of the nanowires at excitation wavelengths from 700 to 800 nm for different values of the gap between the nanowires.

wearable SERS sensor. The Raman peaks at 1016, 1603, and 1637 cm^{-1} correspond to characteristic Raman peaks of ascorbic acid and urea, while the main component of the human sweat other than water is sodium chloride which has no Raman-active molecular vibrations (see Table S1 in the Supporting Information for details). In contrast, no observable Raman peaks from the same human sweat sample were obtained on a silicon wafer. Moreover, we used the wearable SERS sensor to detect urea dissolved in water at various concentrations of 1×10^{-3}, 10×10^{-3}, 100×10^{-3}, and 1 M from 2 μL drops. Figure 5b shows the measured Raman spectra of the urea solutions with the characteristic Raman peak at 1003 cm^{-1} after baseline corrections. Likewise, we obtained Raman spectra of ascorbic acid at minute concentrations of 1×10^{-9}, 10×10^{-9}, 100×10^{-9}, and 1000×10^{-9} M from 2 μL drops with characteristic Raman peaks at 1020, 1200, 1337, 1606, and 1636 cm^{-1}, after baseline corrections (Figure 5c). These results illustrate that the wearable SERS sensor can detect urea and ascorbic acid with low concentrations by comparing them with the human sweat spectra from Figure 5a. These ranges cover the typical concentrations of urea and ascorbic acid on human skin after sweat evaporation, indicating the practical utility of the wearable SERS sensor for sweat analysis on the human skin.

Next, to demonstrate the capability of the wearable SERS sensor for forensic science as another potential application, we performed SERS of some of the widely abused drugs of abuse in the world,[28] including methamphetamine (MA), 3,4-methylenedioxymethamphetamine (MDMA), cocaine, (2-iodophenyl)(1-((1-methylpiperidin-2-yl)methyl)-*1H*-indol-3-yl)methanone (AM2233), morphine, 1-pentyl-3-(1-naphthoyl)indole (JWH-018), triazolam, and zopiclone. One potential application scenario is that the wearable SERS sensor is integrated onto the surfaces of objects frequently touched by drug abusers, such as a plastic lighter, silicon phone case, PET plastic bottle, metal can, and ABS plastic computer keyboard for drug surveillance so that when the drug abusers touch them with their hands contaminated with trace-amount drugs, they can be tracked by virtue of the high sensitivity of the wearable SERS sensor. Specifically, in our demonstration, these drugs were dissolved in methanol and measured on the wearable SERS sensor at concentrations of 0.67×10^{-3} M for methamphetamine, 0.33×10^{-3} M for cocaine, 0.52×10^{-3} M for MDMA, 0.22×10^{-3} M for AM-2233, 0.35×10^{-3} M for morphine, 0.29×10^{-3} M for JWH-018, 0.29×10^{-3} M for triazolam, and 0.26×10^{-3} M for zopiclone. Their Raman spectra with characteristic peaks obtained after baseline subtraction are shown in Figure 5d (see Table S2 in the Supporting Information for details of Raman peak assignments). No Raman signal was obtained at these concentrations on a silicon substrate, which demonstrates the effectiveness of SERS in the detection of drugs of abuse. Furthermore, MDMA dissolved in water was detected at low concentrations of 520×10^{-9} and 5.2×10^{-6} M on the wearable SERS sensor attached to the surfaces of various daily life products, including a plastic lighter, silicon phone case, PET plastic bottle, metal can (aluminum), and ABS plastic computer keyboard as shown in Figure 5e, which confirms the surface-agnostic capability of the wearable SERS sensor. Here, the main Raman peaks of MDMA are at 525, 632, 714, 811, 1245, 1366, 1435, and 1492 cm^{-1} while the other Raman peaks mainly come from the surfaces of the various daily life products where the sensor was attached.

Finally, to demonstrate the capability of the wearable SERS sensor for environmental monitoring, we used it to identify microplastics in water with different concentrations. Specifically, microplastic pollution is known to spread extensively across the oceans on Earth, affecting many ecosystems.[29,30] The most abundant microplastic species found floating in the ocean is polyethylene, constituting approximately 54.5% of all floating microplastic pollution. Figure 5f shows the Raman

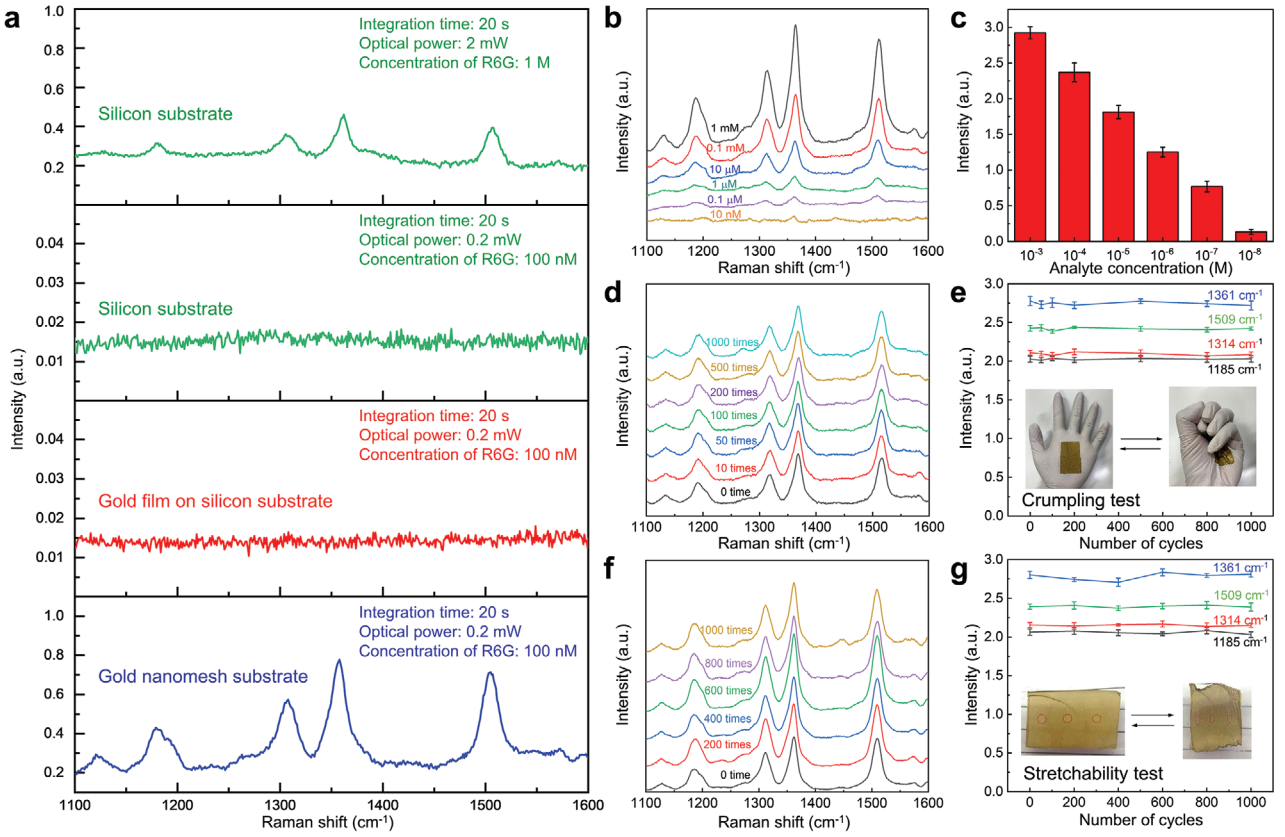

Figure 3. Basic SERS performance of the wearable SERS sensor. a) Raman spectra of R6G molecules on a silicon substrate, gold film substrate, and gold nanomesh substrate obtained under different measurement conditions (e.g., integration time, excitation power, R6G concentration) after baseline subtraction. Excitation wavelength: 785 nm. b) Raman spectra of R6G molecules on the wearable SERS sensor obtained at different R6G concentrations for an integration time of 20 s with an excitation power of 0.2 mW at an excitation wavelength 785 nm after baseline subtraction. c) Intensities of the Raman peaks at a Raman shift of 1361 cm^{-1} at different R6G concentrations, with standard deviations as error bars. The detection limit of the wearable SERS sensor for R6G molecules is about 10×10^{-9} M. d) Raman spectra and e) characteristic Raman peaks of R6G molecules on the gold nanomesh adhered to a glove during the 1000-cycle crumpling test after baseline subtraction, with standard deviations as error bars. The inset shows pictures of the wearable SERS sensor on the glove when the hand was opened and closed. f) Raman spectra and g) characteristic Raman peaks of R6G molecules on the gold nanomesh adhered to a prestretched PDMS substrate during the 1000-cycle stretchability test, with standard deviations as error bars. The inset shows pictures of the wearable SERS sensor on the PDMS substrate when the PDMS substrate was stretched and released. The error bars in panels (c), (e), and (g) are the standard deviations calculated from five different samples.

spectrum of polyethylene microbeads (Figure S2a,b, Supporting Information) in distilled water on a silicon substrate and the wearable SERS sensor. Here, the polyethelene microbeads were aggregated on the liquid surface due to their high hydrophobicity, but some of them remained dispersed in the liquid at a lower concentration. The CC stretch peaks are located at 1063 and 1129 cm^{-1}; the CH_2 twist has its Raman shift at 1296 cm^{-1}; and the CH_2 bend peaks are located at 1416, 1440, and 1463 cm^{-1}.[31] The highest Raman peak that appeared at 1296 cm^{-1} was used for Raman mapping. Figure 5g shows an optical image and Raman map of the wearable SERS sensor attached to a silicon wafer with polyethylene microbeads of density 950 g L^{-3} at a concentration of 0.1%. It is evident from the Raman map that the wearable SERS sensor is robust for the detection of microplastics. Even if the nanomesh structure of the sensor is partially damaged under rough conditions, it can provide reproducible SERS signal enhancements for polyethylene microbeads. In addition, there is no significant difference in measured Raman spectra of dry and wet microplastic samples as long as the microplastics remain in close proximity to the surface of the substrate at the time of SERS measurements. In comparison, a Raman map on a silicon wafer with identical experimental conditions is shown in Figure S2c (Supporting Information), which exhibits a much lower Raman intensity. Moreover, Figure S2d,e (Supporting Information) shows an approach as a potential practical application to evaluating water pollution by attaching the wearable SERS sensor to a water-immersible surface and submerging it for 10 s.

3. Conclusions

In summary, we demonstrated highly scalable, wearable SERS by using an easy-to-fabricate, low-cost, ultrathin, flexible, stretchable, adhesive, and biointegratable gold nanomesh that enabled the detection and identification of diverse analytes at

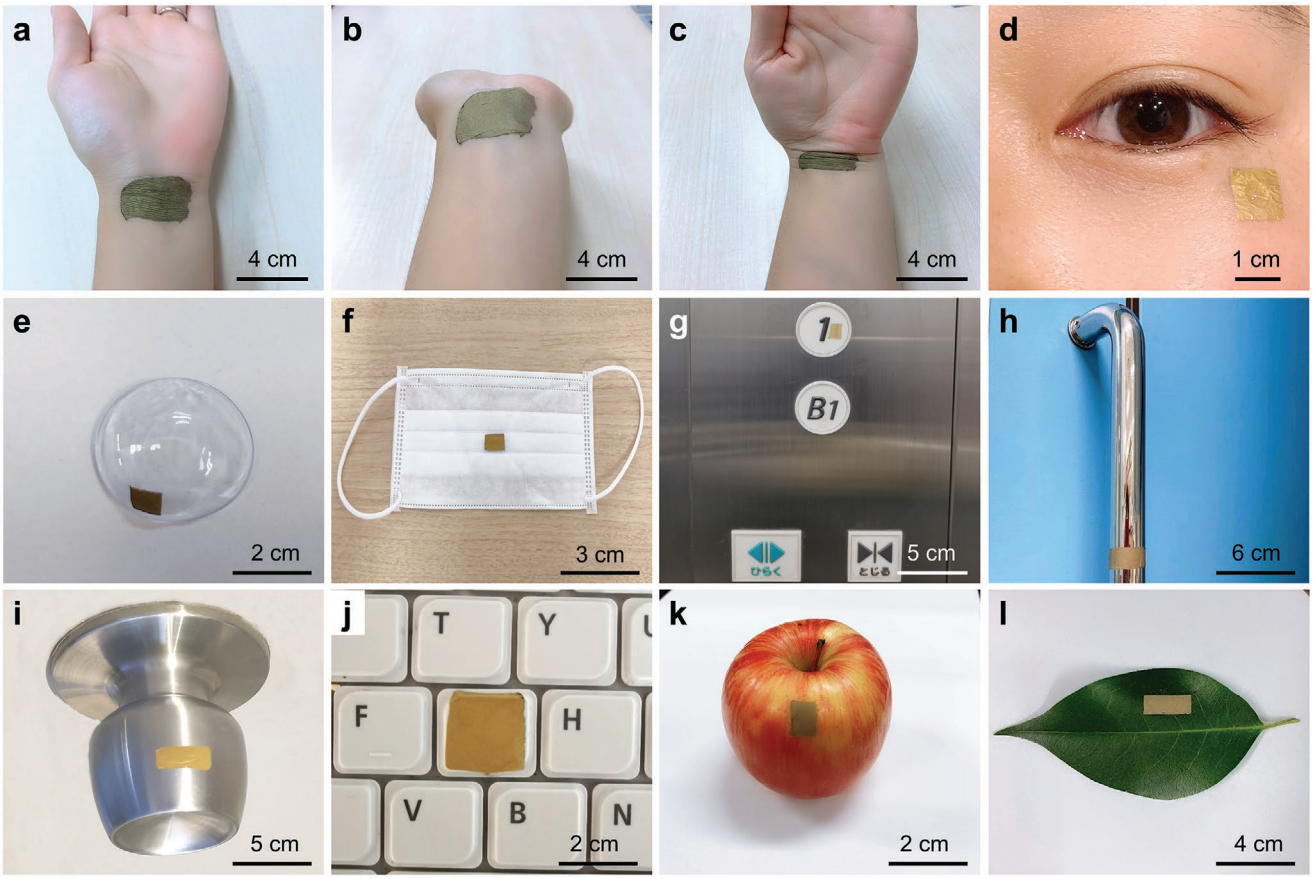

Figure 4. Pictures of the wearable SERS sensor to demonstrate its wearability on metals, plastics, fabrics, and organics for diverse applications. a) Wearable SERS sensor adhered to a human wrist, followed by undergoing b) wrist flexion and c) extension. d,e) Wearable SERS sensor adhered to a human cheek and contact lens to detect biomarkers in tears. f–j) Wearable SERS sensor adhered to a face mask, elevator control panel, door handle, doorknob, and computer keyboard for environmental monitoring and infection surveillance, respectively. k,l) Wearable SERS sensor adhered to an apple and leaf for food safety applications.

low concentrations (10×10^{-9} M for R6G and ascorbic acid solutions) on virtually all arbitrary surfaces. The wearable SERS sensor exhibited excellent practical utility for various types of applications, including the detection of sweat biomarkers, drugs of abuse, and microplastics that were explored in this study. This wearable SERS sensor represents a significant step toward the generalizability and practicality of wearable sensing technology.

There is one limitation to the demonstrated wearable SERS sensor. It requires an external light source to excite Raman scattering of analytes and an external spectrometer to collect scattered light. To make it an independent device, one possible solution is to further integrate a semiconductor nanolaser and a nanospectrometer into the wearable SERS sensor by direct bonding. With this improvement, our wearable SERS sensor is expected to be highly valuable as an essential ingredient of wearable sensing technology.

4. Experimental Section

Chemicals: R6G, PVA powders, and zopiclone were purchased from Sigma Aldrich. The polyethylene microbeads used in this study are the polyethylene nanospheres 0.95 g cc^{-1} 200–9900 nm – 1 g (≈1–10 µm size) from Cospheric LLC. Triazolam, urea (Wako 1st Grade), and ascorbic acid (0.1 M) were purchased from FUJIFILM Wako Pure Chemical Corporation. Deionized water was collected at 15.0 MΩ and 14.6 °C from Milli-Q (Merck Millipore) using vent filters MPK01 and Q-POD1.

Fabrication of the Wearable SERS Sensor: The fabrication process of the wearable SERS sensor and its integration into a target surface are described as follows and shown in Figure 1c. First, a PVA aqueous solution was formed by dissolving 8 wt% PVA into deionized water and stirring at 80 °C for 12 h. Then, PVA nanofibers with a diameter of ≈500 nm were prepared by electrospinning an 8 wt% PVA aqueous solution and intertwined to form a mesh-like sheet by electrospinning at 25 kV for 40 min by using microfluidic pumps at 1 mL h^{-1} flow rate. Second, a 150 nm thick gold layer was thermally deposited on the surface of the PVA nanofibers at a gold flow rate of 0.1 nm s^{-1} at a high vacuum (10^{-6} torr) to produce a gold nanomesh. Finally, water was sprayed on a target surface (e.g., the human skin, leaf, fruit, glove, or face mask) to attach the gold nanomesh on the surface, followed by spraying water again, but on the gold nanomesh to dissolve and rinse away the PVA nanofibers, resulting in a pure gold nanomesh structure without PVA. The attached gold nanomesh was then dried at room temperature.

Raman Measurements: Raman spectra from all the samples except the drugs were obtained using an RM 2000 microscopic confocal Raman spectrometer (InVia, Renishaw PLC, England) excited by a 785 nm wavelength continuous-wave laser with a maximum power

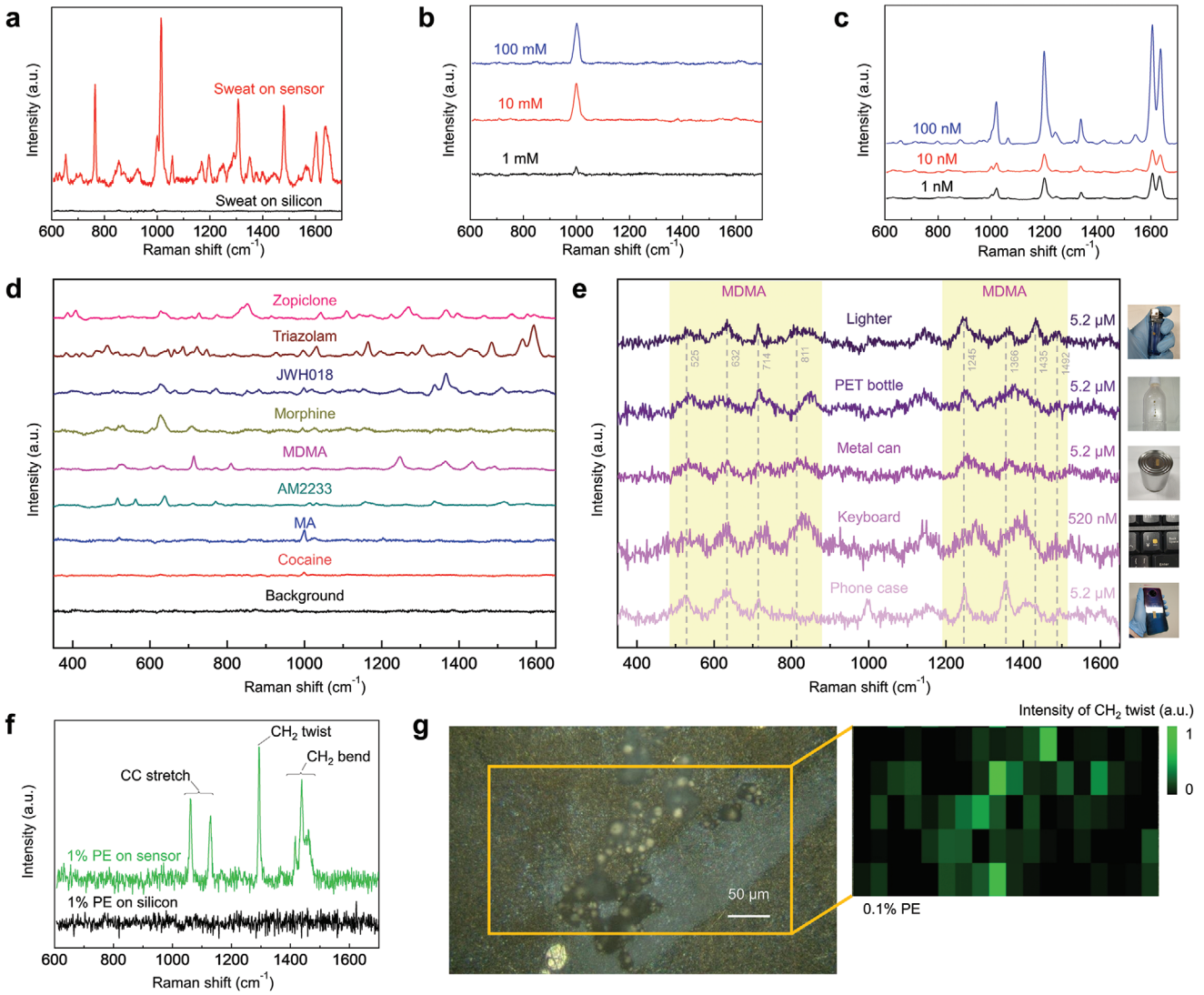

Figure 5. Potential applications of the wearable SERS sensor. a–c) Raman spectra of human sweat, aqueous urea solution, and ascorbic acid aqueous solution, respectively, obtained on the wearable SERS sensor for an integration time of 20 s with an excitation power of 5 mW at an excitation wavelength of 785 nm after baseline subtraction. d) Raman spectra of various drugs of abuse in methanol solution obtained on the wearable SERS sensor for an integration time of 1 s with an excitation power of 10 mW at an excitation wavelength 785 nm after baseline subtraction. e) Raman spectra of MDMA aqueous solution for an integration time of 3 s at an excitation power of 10 mW with eight acquisitions for 5.2×10^{-6} M and for an integration time of 10 s with four acquisitions for 520×10^{-9} M on the wearable SERS sensor attached to the surfaces of various daily life products, including a plastic lighter, silicon phone case, PET plastic bottle, metal can, and ABS plastic computer keyboard. f) Raman spectra of polyethylene microbeads obtained on the wearable SERS sensor and a silicon substrate for an integration time of 20 s with an excitation power of 5 mW at an excitation wavelength of 785 nm after baseline subtraction. g) Raman map (at a Raman shift from 1286 to 1302 cm^{-1}) of polyethylene microbeads obtained on the wearable SERS sensor dispersed in deionized water at a concentration of 0.1% for an integration time of 10 s with an excitation power of 0.5 mW at an excitation wavelength of 785 nm after baseline subtraction.

of 500 mW. The drugs of abuse were evaluated using Laser Raman Microscopy RAMANforce from Nanophoton Corp. The portable spectrometer used in Movie S1 in the Supporting Information is the NanoRam Handheld Raman Spectrometer from B&W Tek. Scanning electron microscope (SEM) images of the wearable SERS sensor fabrication and microplastic particles were taken from a JSM-7600F FESEM microscope. The wearable SERS sensor attached to the glove was worn on a hand for the flexibility test. After opening and closing the hand multiple times, the Raman spectra of R6G on the wearable SERS sensor with the glove were obtained. The stretchability of the wearable SERS sensor was examined on a PDMS substrate, which was prestretched by 50%. When releasing the PDMS substrate, the gold nanomesh formed wrinkled structures and did not break even if it was fully released. The Raman spectra of R6G on the gold nanomesh with the PDMS substrate were obtained at different compression strains in compression cycles (up to 1000 times). The Raman measurements in Figure 3 were performed under 50× magnification for performance characterizations, while those in Figure 5 were conducted under 20× magnification for practical applications.

Material Characterization: Figure 1d–f shows the SEM images corresponding to the PVA nanofibers, PVA/gold nanofibers, and semihollow gold nanofiber, respectively. The diameter of the PVA nanofiber (≈500 nm) and the thickness of the gold layer (150 nm) were optimized to maximize the effect of localized surface plasmon

resonance on the surface of the semihollow gold nanofiber. Figure 1b shows that the wearable SERS sensor can be produced in large areas, while its inset shows the gold nanomesh under an optical microscope using a 50× objective lens.

Human Sweat Samples: The human sweat samples were collected with a micropipette from exercise-induced sweat on the clean skin of a voluntary human subject. The SERS test was approved by the Research Ethics Committee in the Graduate School of Science at the University of Tokyo (approval number: 20–352). The human subject expressed informed consent prior to the sample collection.

Supporting Information

Supporting Information is available from the Wiley Online Library or from the author.

Acknowledgements

This research was supported by MEXT Quantum Leap Flagship Program (JPMXS0120330644), JSPS KAKENHI (JP18K13798, JP20K14785), JSPS Core-to-Core Program, KISTEC, Murata Science Foundation, White Rock Foundation, University of Tokyo GAP Fund, and UTokyo IPC. P.M.P. acknowledges financial support from the Grant-in-Aid for JSPS Fellows (P20789). J.G.P. acknowledges financial support from the JSPS Grant-in-Aid for Young Scientists (20K15227) and the Grant-in-Aid for JSPS Fellows (19F19805).

Conflict of Interest

K.G. is a shareholder of CYBO, Cupido, and LucasLand. T.H.X., L.L., K.H., and K.G. hold a pending patent for the gold nanomesh sensor.

Author Contributions

L.L. and P.M.P. contributed equally to this work. L.L. and P.M.P. are the cofirst authors of this work. L.L. and P.M.P. performed the experiments and analyzed the experimental data. L.L., P.M.P., T.H.X., and K.G. drafted the paper. All coauthors contributed to modifications of the paper. L.L., P.M.P., S.N., and M.M. synthesized the wearable SERS sensors and optimized them. L.L. measured the Raman signals of R6G. L.L. and T.H.X. designed and performed the stretchability and crumping tests. L.L., P.M.P., and T.H.X. took photographs of the wearable SERS sensor on various surfaces. P.M.P., S.K., and T.H.X. designed and analyzed the COMSOL simulations. S.K. performed the COMSOL simulations. P.M.P. designed and performed the experiments with human sweat. P.M.P. and H.S. designed and performed the experiments with drugs using the wearable SERS sensor synthesized by P.M.P. P.M.P., J.G.P., and T.H.X. designed and performed the measurements with microplastics using the wearable SERS sensor synthesized by P.M.P. P.M.P. designed and performed the water immersion test. P.M.P. and S.K. obtained the SEM images. K.H., H.S., Y.K., T.I., and K.T. provided help with the manuscript and data interpretation. T.H.X., J.Q., and K.G. supervised the research project.

Data Availability Statement

The data that support the findings of this study are available from the corresponding author upon reasonable request.

Keywords

drug detection, microplastics, Raman spectroscopy, surface-enhanced Raman spectroscopy, wearable sensors

Received: January 10, 2022
Revised: April 30, 2022
Published online: June 22, 2022

[1] K. Xu, R. Zhou, K. Takei, M. Hong, *Adv. Sci.* **2019**, *6*, 1900925.
[2] E. H. Koh, W.-C. Lee, Y.-J. Choi, J.-I. Moon, J. Jang, S.-G. Park, J. Choo, D.-H. Kim, H. S. Jung, *ACS Appl. Mater. Interfaces* **2021**, *13*, 3024.
[3] Y. Khan, A. E. Ostfeld, C. M. Lochner, A. Pierre, A. C. Arias, *Adv. Mater.* **2016**, *28*, 4373.
[4] D. R. Seshadri, R. T. Li, J. E. Voos, J. R. Rowbottom, C. M. Alfes, C. A. Zorman, C. K. Drummond, *npj Digital Med.* **2019**, *2*, 72.
[5] J. Kim, A. S. Campbell, B. E.-F. de Ávila, J. Wang, *Nat. Biotechnol.* **2019**, *37*, 389.
[6] Z. Sonner, E. Wilder, J. Heikenfeld, G. Kasting, F. Beyette, D. Swaile, F. Sherman, J. Joyce, J. Hagen, N. Kelley-Loughnane, R. Naik, *Biomicrofluidics* **2015**, *9*, 031301.
[7] W. Gao, H. Ota, D. Kiriya, K. Takei, A. Javey, *Acc. Chem. Res.* **2019**, *52*, 523.
[8] J. Langer, D. Jimenez de Aberasturi, J. Aizpurua, R. A. Alvarez-Puebla, B. Auguié, J. J. Baumberg, G. C. Bazan, S. E. J. Bell, A. Boisen, A. G. Brolo, J. Choo, D. Cialla-May, V. Deckert, L. Fabris, K. Faulds, F. J. García de Abajo, R. Goodacre, D. Graham, A. J. Haes, C. L. Haynes, C. Huck, T. Itoh, M. Käll, J. Kneipp, N. A. Kotov, H. Kuang, E. C. Le Ru, H. K. Lee, J.-F. Li, X. Y. Ling, et al., *ACS Nano* **2020**, *14*, 28.
[9] C. Matricardi, C. Hanske, J. L. Garcia-Pomar, J. Langer, A. Mihi, L. M. Liz-Marzán, *ACS Nano* **2018**, *12*, 8531.
[10] A. Shiohara, J. Langer, L. Polavarapu, L. M. Liz-Marzán, *Nanoscale* **2014**, *6*, 9817.
[11] D. Jimenez de Aberasturi, A. B. Serrano-Montes, J. Langer, M. Henriksen-Lacey, W. J. Parak, L. M. Liz-Marzán, *Chem. Mater.* **2016**, *28*, 6779.
[12] N. Chen, T.-H. Xiao, Z. Luo, Y. Kitahama, K. Hiramatsu, N. Kishimoto, T. Itoh, Z. Cheng, K. Goda, *Nat. Commun.* **2020**, *11*, 4772.
[13] W. Yingli, Z. Chen, W. Jingjing, L. Xuan, X. Lijuan, Z. Shijie, K. Jongmin, W. Xiaozhi, L. Xiangjiang, Y. Yibin, *Sci. Adv.* **2021**, *7*, eabe4553.
[14] J. W. Jeong, S. R. Yang, Y. H. Hur, S. W. Kim, K. M. Baek, S. Yim, H.-I. Jang, J. H. Park, S. Y. Lee, C.-O. Park, Y. S. Jung, *Nat. Commun.* **2014**, *5*, 5387.
[15] J. W. Jeong, M. M. P. Arnob, K.-M. Baek, S. Y. Lee, W.-C. Shih, Y. S. Jung, *Adv. Mater.* **2016**, *28*, 8695.
[16] A. Garg, W. Nam, W. Zhou, *ACS Appl. Mater. Interfaces* **2020**, *12*, 56290.
[17] A. Miyamoto, S. Lee, N. F. Cooray, S. Lee, M. Mori, N. Matsuhisa, H. Jin, L. Yoda, T. Yokota, A. Itoh, M. Sekino, H. Kawasaki, T. Ebihara, M. Amagai, T. Someya, *Nat. Nanotechnol.* **2017**, *12*, 907.
[18] S. Hagan, E. Martin, A. Enríquez-de-Salamanca, *EPMA J.* **2016**, *7*, 15.
[19] M. Tamhane, S. Cabrera-Ghayouri, G. Abelian, V. Viswanath, *Pharm. Res.* **2019**, *36*, 40.
[20] L. W. Chan, M. N. Anahtar, T.-H. Ong, K. E. Hern, R. R. Kunz, S. N. Bhatia, *Nat. Nanotechnol.* **2020**, *15*, 792.
[21] M. Phillips, V. Basa-Dalay, G. Bothamley, R. N. Cataneo, P. K. Lam, M. P. R. Natividad, P. Schmitt, J. Wai, *Tuberculosis* **2010**, *90*, 145.

[22] Y. Saalberg, M. Wolff, *Clin. Chim. Acta* **2016**, *459*, 5.
[23] D. M. Ruszkiewicz, D. Sanders, R. O'Brien, F. Hempel, M. J. Reed, A. C. Riepe, K. Bailie, E. Brodrick, K. Darnley, R. Ellerkmann, O. Mueller, A. Skarysz, M. Truss, T. Wortelmann, S. Yordanov, C. L. P. Thomas, B. Schaaf, M. Eddleston, *eClinicalMedicine* **2020**, *29*, 100609.
[24] N. Huang, P. Pérez, T. Kato, Y. Mikami, K. Okuda, R. C. Gilmore, C. D. Conde, B. Gasmi, S. Stein, M. Beach, E. Pelayo, J. O. Maldonado, B. A. Lafont, S.-I. Jang, N. Nasir, R. J. Padilla, V. A. Murrah, R. Maile, W. Lovell, S. M. Wallet, N. M. Bowman, S. L. Meinig, M. C. Wolfgang, S. N. Choudhury, M. Novotny, B. D. Aevermann, R. H. Scheuermann, G. Cannon, C. W. Anderson, R. E. Lee, et al., *Nat. Med.* **2021**, *27*, 892.
[25] G. P. Hancke, B. de C. E. Silva, G. P. HanckeJr, *Sensors* **2012**, *13*, 393.
[26] M. Fan, Z. Zhang, J. Hu, F. Cheng, C. Wang, C. Tang, J. Lin, A. G. Brolo, H. Zhan, *Mater. Lett.* **2014**, *133*, 57.
[27] X. Wang, X. Zhu, Y. Chen, M. Zheng, Q. Xiang, Z. Tang, G. Zhang, H. Duan, *ACS Appl. Mater. Interfaces* **2017**, *9*, 31102.
[28] S. Odoardi, V. Valentini, N. De Giovanni, V. L. Pascali, S. Strano-Rossi, *Microchem. J.* **2017**, *133*, 302.
[29] A. A. Koelmans, N. H. Mohamed Nor, E. Hermsen, M. Kooi, S. M. Mintenig, J. De France, *Water Res.* **2019**, *155*, 410.
[30] R. Coyle, G. Hardiman, K. O. Driscoll, *Case Stud. Chem. Environ. Eng.* **2020**, *2*, 100010.
[31] J. Fischer, G. M. Wallner, A. Pieber, *Macromol. Symp.* **2008**, *265*, 28.